

Muon $g-2$ and searches for a new leptophobic sub-GeV dark boson in a missing-energy experiment at CERN

S.N. Gninenko¹, N.V. Krasnikov^{1,2}, and V.A. Matveev^{1,2}

¹ *Institute for Nuclear Research of the Russian Academy of Sciences, 117312 Moscow, Russia*

² *Joint Institute for Nuclear Research, 141980 Dubna, Russia*

(Dated: May 12, 2015)

The 3.6σ discrepancy between the predicted and measured values of the anomalous magnetic moment of positive muons can be explained by the existence of a new dark boson Z_μ with a mass in the sub-GeV range, which is coupled predominantly to the second and third lepton generations through the $L_\mu - L_\tau$ current. After a discussion of the present phenomenological bounds on the Z_μ coupling, we show that if the Z_μ exists, it could be observed in the reaction $\mu + Z \rightarrow \mu + Z + Z_\mu$ of a muon scattering off nuclei by looking for an excess of events with large missing muon beam energy in a detector due to the prompt bremsstrahlung Z_μ decay $Z_\mu \rightarrow \nu\nu$ into a couple of neutrinos. We describe the experimental technique and the preliminary study of the feasibility for the proposed search. We show that this specific signal allows for a search for the Z_μ with a sensitivity in the coupling constant $\alpha_\mu \gtrsim 10^{-11}$, which is 3 orders of magnitude higher than the value required to explain the discrepancy. We point out that the availability of high-energy and -intensity muon beams at CERN SPS provides unique opportunity to either discover or rule out the Z_μ in the proposed search in the near future. The experiment is based on the missing-energy approach developed for the searches for invisible decays of dark photons and (pseudo)scalar mesons at CERN and is complementary to these experiments.

PACS numbers: 14.80.-j, 12.60.-i, 13.20.Cz, 13.35.Hb

I. INTRODUCTION

The precise measurement of the anomalous magnetic moment of the positive muon $a_\mu = (g-2)/2$ from the Brookhaven AGS experiment 821 [1] gives a result which is about 3.6σ higher than the Standard Model (SM) prediction

$$a_\mu^{exp} - a_\mu^{SM} = 288(80) \times 10^{-11} \quad (1)$$

This result may signal the existence of new physics beyond the Standard Model. At present the most popular explanation of this discrepancy is supersymmetry with a chargino and sneutrino lighter than 800 GeV [2]. Other possible explanations include leptoquarks [3] or some exotic flavor-changing interactions [4]. All of these explanations assume the existence of new heavy particles with masses $\geq O(100)$ GeV. Another explanation of the $g-2$ anomaly is related to the existence of a new light (with a mass $m_{Z'} \leq O(1)$ GeV) vector boson (dark photon) which couples very weakly with the muon with $\alpha_{Z'} \sim O(10^{-8})$ [5]–[10], see also Ref. [11].

In this paper we consider the muon $g-2$ anomaly as an indication for the existence of the new light vector boson Z_μ , which is coupled predominantly to the second and third lepton generations. We propose an experiment to search for the Z_μ in the high-energy muon beam at the CERN SPS. If the Z_μ exists, it could be observed in the reaction $\mu + Z \rightarrow \mu + Z + Z_\mu$ of a high-energy muon scattering off nuclei by looking for an excess of events with a specific signature, namely large missing muon beam energy in the detector. The experiment uses the missing-energy approach developed for the search for invisible decays of dark photons and (pseudo)scalar mesons at

CERN [12–14] and is complementary to these proposals.

The rest of the paper is organized in the following way. The existing bounds are discussed in Sec. II. In Sec. III the Z_μ production and decay modes are described. The method of the search and the experimental setup are presented in Sec. IV, background sources are discussed in Sec. V, and the expected sensitivity is shown in Sec. VI. Section VII contains concluding remarks.

II. PHENOMENOLOGY AND EXISTING EXPERIMENTAL BOUNDS

As discussed in the Introduction one of the possible explanations of the $g_\mu - 2$ anomaly assumes the existence of a new light vector boson Z' which interacts with muons like a photon, namely

$$L_{Z'} = e' \bar{\mu} \gamma_\nu \mu Z'^\nu. \quad (2)$$

The interaction (2) gives additional contribution to the muon anomalous magnetic moment $a_\mu \equiv \frac{g_\mu - 2}{2}$

$$a'_l = \frac{\alpha'}{\pi} \int_0^1 \frac{x^2(1-x)}{x^2 + (1-x)M_{Z'}^2/m_l^2}, \quad (3)$$

where $\alpha' = (e')^2/4\pi$ and $M_{Z'}$ is the mass of the Z' boson. Equation (3) allows one to determine the α_μ which explains the $g_\mu - 2$ anomaly. For $M_{Z'} \ll m_\mu$ we find from Eq.(1) that

$$\alpha' = (1.8 \pm 0.5) \times 10^{-8} \quad (4)$$

For another limiting case $M_{Z'} \gg m_\mu$ Eq.(1) leads to

$$\alpha' \frac{m_\mu^2}{M_{Z'}^2} = (2.7 \pm 0.8) \times 10^{-8} \quad (5)$$

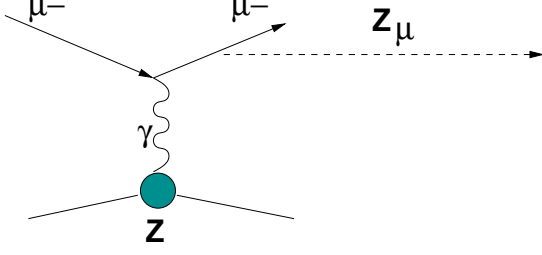


FIG. 1: Diagram illustrating the massive Z_μ production in the reaction $\mu + Z \rightarrow \mu + Z + Z_\mu$ of muons scattering off a nuclei (A,Z). The Z_μ is either stable or it decays invisibly if its mass $M_{Z_\mu} \leq 2m_\mu$, or (as shown) it could subsequently decay into a $\mu^+\mu^-$ pair if $M_{Z_\mu} > 2m_\mu$.

But the postulation of the interaction (2) of the Z' boson with a muon is not the end of the story. The main question is, what about the interaction of the Z' boson with other quarks and leptons? There are a lot of possibilities here. For instance, a very popular scenario involves an interaction of the Z' boson with quarks and leptons that is proportional to the electromagnetic current J_ν of the SM, namely

$$L_{Z'} = e' J_\nu Z'^\nu. \quad (6)$$

The natural realization of this scenario is the existence of a new gauge boson Z' which interacts with the SM fields through the mixing with the SM hypercharge [15, 16]

$$\Delta L = \frac{\epsilon}{2} F^{Y,\alpha\beta} F_{\alpha\beta}^{Z'}. \quad (7)$$

For the scenario with the interaction (6) of the Z' boson with the electromagnetic current of the SM there are several interesting constraints. Bounds [17, 18] from the electron magnetic moment value

$$\Delta a_e = a_e^{\text{exp}} - a_e^{\text{SM}} = -1.06(0.82) \times 10^{-12} \quad (8)$$

exclude the region $M_{Z'} < 30$ MeV. Other experiments use dilepton resonance searches, $Z_\mu \rightarrow l^+l^-$. First we consider the bounds obtained under the assumption that the Z' boson decays mainly into charged leptons, i.e. $\text{Br}(Z' \rightarrow l^+l^-) = 1$, with $l = e, \mu$. The Phenix Collaboration looked for the Z' boson in $\pi^0, \eta \rightarrow (Z' \rightarrow e^+e^-)\gamma$ decays and excluded the masses $36 < M_{Z'} < 90$ MeV [19]. The A1 Collaboration used the reaction $eZ \rightarrow eZ'Z; Z' \rightarrow e^+e^-$ to search for the Z' boson and excluded the masses $40 < M_{Z'} < 300$ MeV [20]. The BABAR Collaboration looked for the Z_μ boson in the reaction $e^+e^- \rightarrow \gamma Z', Z' \rightarrow e^+e^-, \mu^+\mu^-$ and excluded the masses $30 \text{ MeV} < M_{Z'} < 10.2 \text{ GeV}$ [21]. Finally, taking into account the recent results from K -decay experiments [22], the possibility of the $g-2$ explanation in the model with the interaction (6) of the Z' boson with the assumption that $\text{Br}(Z' \rightarrow l^+l^-) = 1$ is excluded, see, e.g. Ref.[23] for a discussion.

For the model with the interaction (6) there is the possibility that the Z' boson decays dominantly invisibly into new light particles χ with the branching $\text{Br}(Z' \rightarrow \chi\bar{\chi}) = 1$. For this scenario the $K^+ \rightarrow \pi^+ + \text{missing energy}$ bound [24] and the off-resonance BABAR result [25] exclude a sizable parameter space, except for $30 < M_{Z'} < 50$ MeV and the narrow region around $M_{Z'} = 140$ MeV [26], [27].

Another interesting scenario is that from Ref. [27], where the light gauge boson (the dark leptonic gauge boson) interacts with the leptonic current, namely

$$L_{Z'} = e' [\bar{e}\gamma_\nu e + \bar{\nu}_{eL}\gamma_\nu \nu_{eL} + \bar{\mu}\gamma_\nu \mu + \bar{\nu}_{\mu L}\gamma_\nu \nu_{\mu L} + \bar{\tau}\gamma_\nu \tau + \bar{\nu}_{\tau L}\gamma_\nu \nu_{\tau L}] Z'^\nu \quad (9)$$

This interaction does not contain quarks and as a consequence the corresponding model escapes many quarkonium-decay constraints [27]. The relevant searches for the dark leptonic gauge boson include fixed-target [20] and neutrino trident experiments [28, 29], the BABAR search for $e^+e^- \rightarrow \gamma + \text{missing energy}$ [21], beam-dump experiments [30–32], and last but not least the Borexino experiment [33]. It appears that for the model with the dark leptonic gauge boson the most restrictive bound comes from the Borexino experiment [33]. The presence of a new vector boson would alter the charged-current interaction between solar ν_e neutrinos and target electrons in the detector. The bounds from the 862 KeV ^7Be solar neutrino flux measurement at the Borexino experiment excludes the possibility that the leptonic gauge boson can explain the $g_\mu - 2$ anomaly [34], see Fig. 3 in Ref.[27] where constraints on the parameter space of the dark lepton gauge boson model were presented [51].

In Refs. [5] - [7], an explanation of the $g_\mu - 2$ anomaly was given by a model where the new light gauge boson (hereafter denoted as Z_μ) interacts with the $L_\mu - L_\tau$ current as

$$L_{Z_\mu} = e_\mu [\bar{\mu}\gamma_\nu \mu + \bar{\nu}_{\mu L}\gamma_\nu \nu_{\mu L} - \bar{\tau}\gamma_\nu \tau - \bar{\nu}_{\tau L}\gamma_\nu \nu_{\tau L}] Z_\mu^\nu \quad (10)$$

which is anomaly free and corresponds to the global flavor symmetry $U(1)_{L_\mu - L_\tau}$ which commutes with the SM $SU_c(3) \otimes SU(2)_L \otimes U(1)_Y$ gauge group [35]. In addition, it was recently shown that the Z_μ with a mass $\simeq 2$ MeV can explain the gap in the cosmic neutrino spectrum observed by the IceCube Collaboration [36].

As the Z_μ does not couple to quarks, electrons and ν_e neutrinos, it escapes the most current experimental constraints. The most restrictive bound comes from the results of experiments on neutrino trident production $\nu_\mu N \rightarrow \nu_\mu N + \mu^+\mu^-$ [28, 29]. As was shown in Ref. [37] that the CCFR data [29] on $\nu_\mu N \rightarrow \nu_\mu N + \mu^+\mu^-$ production exclude the $g_\mu - 2$ explanation for a Z_μ -boson mass $m_{Z_\mu} \geq 400$ MeV.

We note that at the one-loop level the Z_μ and the photon are kinetically mixed. The effective coupling of Z_μ to electrons (or quarks) due to the muon or τ -lepton loop is $\simeq O(\frac{\alpha}{\pi})e_\mu$, i.e. it is suppressed by at least a factor $\simeq 3 \cdot 10^{-3}$. This results in rather modest constraints on

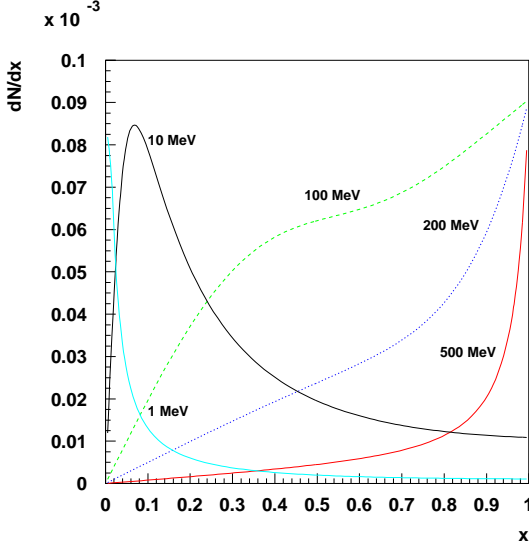


FIG. 2: Calculated distributions of the Z_μ fractional energy $x = E_{Z_\mu}/E_\mu$ from the reaction $\mu + Z \rightarrow \mu + Z + Z_\mu$ at a muon beam energy $E_\mu = 150$ GeV for different Z_μ masses indicated near the curves. The spectra are normalized to a common maximum.

invisible decays of Z_μ which one can extract from dark-photon and other experiments. For example, the bound on the coupling α_μ from the $K^+ \rightarrow \pi^+ + \text{missing energy}$ decay is at the level $\alpha_\mu \leq O(10^{-3})$, which is several orders of magnitude below the value from Eq.(4). The visible decay $Z_\mu \rightarrow e^+e^-$ can also occur at the one-loop level. Its branching fraction is estimated to be $\text{Br}(Z_\mu \rightarrow e^+e^-) = O((\frac{\alpha}{\pi})^2 \alpha_\mu) = O(10^{-5})\alpha_\mu$. As a consequence, in any experiment using electrons or quarks as a source of Z_μ 's, the number of $Z_\mu \rightarrow e^+e^-$ signal events is suppressed by a factor $O((\frac{\alpha}{\pi})^4) \approx 10^{-10}$, resulting in a very weak bound on α_μ (here, the factor $(\frac{\alpha}{\pi})^2$ comes from the Z_μ production). Finally, we note that if the Z_μ couples to light dark matter, then an additional contribution from the invisible decay mode $Z_\mu \rightarrow \text{dark matter}$ that increases the $Z_\mu \rightarrow \text{invisible}$ decay rate is possible. Such a scenario requires additional study, which is beyond the scope of this work.

To conclude this section, let us stress that existing experimental data restrict the explanation of the $g_\mu - 2$ anomaly due to existence of new light gauge boson rather strongly, but they do not completely eliminate it. For the model with the interaction (6) the realization with invisible Z_μ -boson decays into new light χ -particles for $M_{Z_\mu} = 30 - 50$ MeV and around $M_{Z_\mu} = 140$ MeV is still possible. Moreover for the interaction of the Z_μ boson with $L_\mu - L_\tau$ current bounds are rather weak, and a light Z_μ -boson with a mass $M_{Z_\mu} \leq 400$ MeV is not excluded as the source of the $g_\mu - 2$ discrepancy.

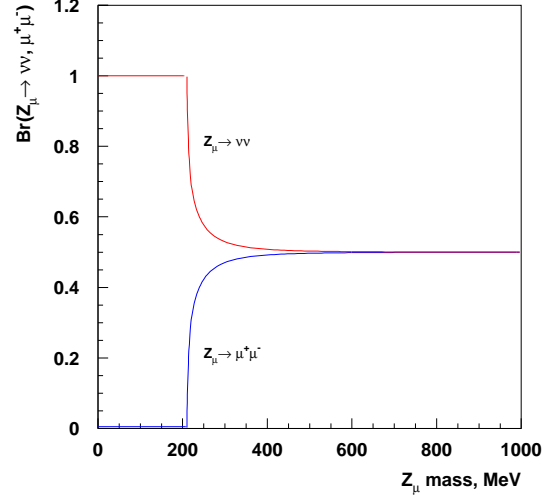


FIG. 3: The branching fraction of the decays $\text{Br}(Z_\mu \rightarrow \nu\nu)$ and $\text{Br}(Z_\mu \rightarrow \mu^+\mu^-)$ as a function of the Z_μ mass.

III. THE Z_μ PRODUCTION AND DECAYS

As the source of Z_μ s, we use bremsstrahlung Z_μ 's produced in the reaction

$$\mu(p) + Z(P) \rightarrow Z(P') + \mu(p') + Z_\mu(k) \quad (11)$$

of high-energy muons scattering off the nuclei of a target, as shown in Fig. 1. Here p, P, P', p', k are the four-momenta of incoming muon, incoming Z nuclei, outgoing Z nuclei, outgoing muon and outgoing Z_μ boson, respectively. In this section we give the main formulas for the production of the Z_μ boson in the reaction of Eq.(11). In the Weizsacker-Williams approximation [38], in the rest frame of the nuclei ($P = (M, 0)$, $p = (E_0, \vec{p})$, $p' = (E', \vec{p}')$, and $k = (E_{Z_\mu}, \vec{k})$), the Z_μ -production cross section at the nuclei

$$\frac{d\sigma(\mu + Z \rightarrow \mu + Z_\mu + Z)}{dE_{Z_\mu} d\cos\theta_{Z_\mu}} \quad (12)$$

is related to the cross section for real photon scattering, $\mu(p)\gamma(q) \rightarrow \mu(p')Z_\mu(k)$ with $q = P' - P$; namely, the following formula applies:

$$\frac{d\sigma(\mu + Z \rightarrow \mu + Z_\mu + Z)}{dE_{Z_\mu} d\cos\theta_{Z_\mu}} = \frac{\alpha\chi}{\pi} \frac{E_0 x \beta_{Z_\mu}}{1-x} \times \frac{d\sigma(p + q \rightarrow p' + k)}{d(pk)} \Big|_{t=t_{min}} \quad (13)$$

Here

$$x \equiv E_{Z_\mu}/E_0, \quad (14)$$

$$t \equiv -q^2, \quad (15)$$

$$\beta_{Z_\mu} = \sqrt{(1 - m_{Z_\mu}^2/E_0^2)} \quad (16)$$

and χ is the effective flux of photons integrated from $t = t_{min}$ to t_{max} [38]. The kinematics is determined at $t = t_{min}$. For a given Z_μ momentum the virtuality t has its minimum value t_{min} when \vec{k} is collinear with the three-vector $\vec{k} - \vec{p}$ [39]. One can find [39] that

$$q^0 = \frac{|\vec{q}|^2}{2M} \approx 0, \quad (17)$$

$$|\vec{q}| = \frac{U}{2E_0(1-x)}, \quad (18)$$

where

$$U \equiv U(x, \theta_{Z_\mu}) = E_0^2 \theta_{Z_\mu}^2 x + m_{Z_\mu}^2 \frac{1-x}{x} + m_\mu^2 x \quad (19)$$

The Mandelstam variables at $t = t_{min}$ have the form [39]

$$-\tilde{u} = m_\mu^2 - u_2 = 2p \cdot k - m_{Z_\mu}^2 = U, \quad (20)$$

$$\tilde{s} = -m_\mu^2 + s_2 = 2p' \cdot k + m_{Z_\mu}^2 = \frac{U}{1-x}, \quad (21)$$

$$t_2 = (p - p')^2 = -\frac{Ux}{1-x} + m_{Z_\mu}^2. \quad (22)$$

For the case of a muon beam (contrary to Ref.[39] where an electron beam was studied) we cannot neglect the muon mass compared to the Z_μ mass and the $2 \rightarrow 2$ differential cross section has the form

$$\begin{aligned} \frac{d\sigma}{dt_2} = & \frac{2\pi\alpha\alpha_\mu}{\tilde{s}^2} \left[\frac{\tilde{s}}{-\tilde{u}} + \frac{-\tilde{u}}{\tilde{s}} + 4\left(\frac{m_\mu^2}{\tilde{s}} + \frac{m_\mu^2}{\tilde{u}}\right)^2 + 4\left(\frac{m_\mu^2}{\tilde{s}} + \frac{m_\mu^2}{\tilde{u}}\right) \right. \\ & \left. + \frac{2m_{Z_\mu}^2 t_2}{-\tilde{u}\tilde{s}} + 2m_{Z_\mu}^2 m_\mu^2 \left(\left(\frac{1}{\tilde{s}}\right)^2 + \left(\frac{1}{\tilde{u}}\right)^2\right) \right]. \end{aligned} \quad (23)$$

In the Weizsacker-Williams approximation the cross section of the $\mu(p) + Z(P) \rightarrow Z(P') + \mu(p') + Z_\mu(k)$ reaction is given by

$$\frac{1}{E_0^2 x} \frac{d\sigma}{dx d\cos\theta_{Z_\mu}} = 4 \left(\frac{\alpha^2 \alpha_\mu \chi \beta_{Z_\mu}}{1-x} \right) \left[\frac{C_2}{U^2} + \frac{C_3}{U^3} + \frac{C_4}{U^4} \right], \quad (24)$$

where

$$C_2 = (1-x) + (1-x)^3, \quad (25)$$

$$C_3 = -2x(1-x)^2 m_{Z_\mu}^2 - 4m_\mu^2 x(1-x)^2, \quad (26)$$

$$C_4 = 2m_{Z_\mu}^4 (1-x)^3 + (1-x)^2 [4m_\mu^4 x^2 + 2m_\mu^2 m_{Z_\mu}^2 (x^2 + (1-x)^2)]. \quad (27)$$

By integrating with respect to θ_{Z_μ} , we find that

$$\frac{d\sigma}{dx} = 2 \left(\frac{\alpha^2 \alpha_\mu \chi \beta_{Z_\mu}}{1-x} \right) \left[\frac{C_2}{V} + \frac{C_3}{2V^2} + \frac{C_4}{3V^3} \right], \quad (28)$$

where

$$V = U(x, \theta_{Z_\mu} = 0) = m_{Z_\mu}^2 \frac{1-x}{x} + m_\mu^2 x \quad (29)$$

For a general electric form factor $G_2(t)$ [38], the effective flux of photons χ is

$$\chi = \int_{t_{min}}^{t_{max}} dt \frac{(t - t_{min})}{t^2} G_2(t). \quad (30)$$

Note that for heavy atomic nuclei A we also have to take into account the inelastic nuclear form factor. Numerically, $\chi = Z^2 \cdot \text{Log}$, where the function Log depends weakly on atomic screening, nuclear size effects and kinematics [39]. Numerically, $\text{Log} \approx (5 - 10)$ for $m_{Z_\mu} \leq 500$ MeV [38, 39]. One can see that compared to the photon bremsstrahlung rate, the Z_μ production rate is suppressed by a factor $\simeq \alpha_\mu m_\mu^2 / \alpha M_{Z_\mu}^2$.

In Fig. 2 an example of the expected distributions of the energy of a Z_μ produced by a 150 GeV muon impinging on the Pb target is shown for different Z_μ masses. The spectra are calculated for the coupling $\alpha_\mu = \alpha$. One can see, that for masses $M_{Z_\mu} \gtrsim 100$ MeV the Z_μ bremsstrahlung distribution is peaked at the maximal beam energy.

For $M_{Z_\mu} < 2m_\mu$ the decays $Z_\mu \rightarrow \mu\bar{\mu}$ are prohibited and the Z_μ decays mainly into $Z_\mu \rightarrow \nu_\mu \bar{\nu}_\mu, \nu_\tau \bar{\nu}_\tau$. For $2m_\mu < M_{Z_\mu} < 2m_\tau$, in addition to decays into neutrino pairs Z_μ also decays into $\mu^+ \mu^-$ pairs with the decay width

$$\Gamma(Z_\mu \rightarrow \mu^- \mu^+) = \frac{\alpha_\mu M_{Z_\mu}}{3} \left(1 + \frac{2m_\mu^2}{M_{Z_\mu}^2} \right) \sqrt{1 - 4 \frac{m_\mu^2}{M_{Z_\mu}^2}} \quad (31)$$

The branching ratio into $\mu^- \mu^+$ pairs is determined by the formula

$$\text{Br}(Z_\mu \rightarrow \mu^- \mu^+) = \frac{K(\frac{m_\mu}{M_{Z_\mu}})}{1 + K(\frac{m_\mu}{M_{Z_\mu}})}, \quad (32)$$

where

$$K(\frac{m_\mu}{M_{Z_\mu}}) = \left(1 + \frac{2m_\mu^2}{M_{Z_\mu}^2} \right) \cdot \sqrt{1 - 4 \frac{m_\mu^2}{M_{Z_\mu}^2}}. \quad (33)$$

For the coupling of Eqs.(4) and (5), the Z_μ with the mass $M_{Z_\mu} \gtrsim 100$ MeV is a short-lived particle with the lifetime $\tau_{Z_\mu} \lesssim 10^{-15}$ s. In Fig. 3 the branching fraction of the decays $Z_\mu \rightarrow \nu\nu$ and $Z_\mu \rightarrow \mu^+ \mu^-$ are shown as functions of the Z_μ mass. One can see that for $M_{Z_\mu} \gtrsim 2m_\mu$, 50% of the Z_μ 's decay invisibly into a couple of neutrinos, while another 50% decay into a $\mu^+ \mu^-$ pair. The latter would result in the muon trident signature in the detector. For Z_μ energies $E_{Z_\mu} \simeq 100$ GeV, the opening angle $\Theta_{\mu^+ \mu^-} \simeq M_{Z_\mu}/E_{Z_\mu}$ of the decay $\mu^+ \mu^-$ pair is still big enough and the decay muons could be resolved in two separated tracks, so the pairs would be mostly detected as double-track events. However, the main problem for the search for the $Z_\mu \rightarrow \mu^+ \mu^-$ decay is the background of muon trident events from the QED reaction

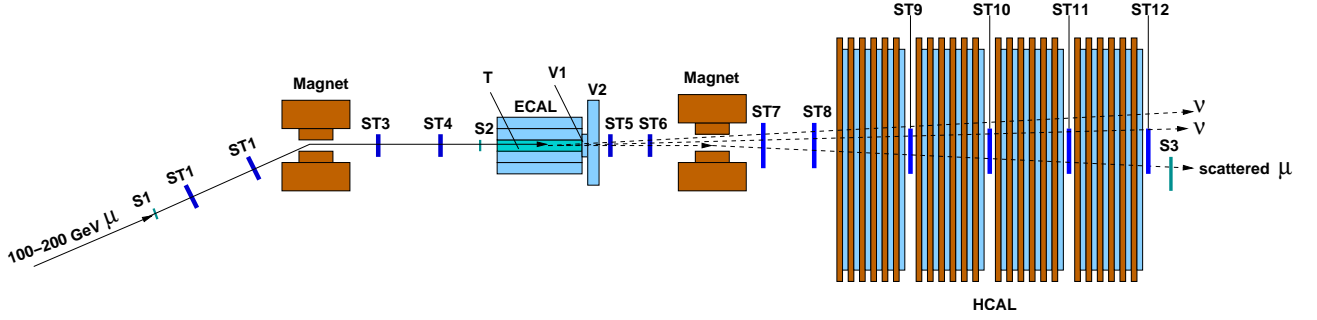


FIG. 4: Schematic illustration of the setup to search for dark Z_μ . The bremsstrahlung Z_μ s are produced in the forward direction in the reaction $\mu + Z \rightarrow \mu + Z + Z_\mu$ of a high-energy muon scattering off nuclei of an active target T . The target is surrounded by an ECAL serving as a veto against photons or other secondaries emitted at a large angle. A fraction $f \lesssim 0.7$, of the primary beam energy is carried away by the scattered muon, while the rest of the total energy is transmitted by the Z_μ decay neutrino through the T , the veto counters V1 and V2, and a massive hermetic HCAL. The neutrino from the $Z_\mu \rightarrow \nu\nu$ decay penetrates them without interactions resulting in a zero-energy signature in the detector. The dashed line represents the trajectory of the outgoing muon which passes through the central HCAL cell without interactions. The momentum of the incident muon is measured by a magnetic spectrometer, while the momentum of the scattered muon is measured by the second one, located downstream of the ECAL (see text).

$\mu Z \rightarrow \mu Z \mu^+ \mu^-$, whose rate substantially exceeds the rate of the reaction (11). An additional study, which is beyond the scope of this work, is required for this decay channel. Here, we mostly focus on the case when the reaction (11) is accompanied by the decay $Z_\mu \rightarrow \nu\nu$, resulting in the invisible final state.

IV. THE EXPERIMENT TO SEARCH FOR THE $\mu + Z \rightarrow \mu + Z + Z_\mu, Z_\mu \rightarrow \nu\nu$

The reaction of the Z_μ production is a rare event. For the previously mentioned parameter space, it is expected to occur with the rate $\lesssim \alpha_\mu/\alpha \sim 10^{-6}$ with respect to the ordinary photon production rate. Hence, its observation presents a challenge for the detector design and performance.

The experimental setup specifically designed to search for the Z_μ production and subsequent decay $Z_\mu \rightarrow \nu\nu$ from the reaction of Eq. (11) of high-energy muon scattering off nuclei in a high density target T is schematically shown in Fig. 4. The experiment could employ the upgraded muon beam at the CERN SPS described in details in Ref.[40]. The beam was designed to transport high fluxes of muons of the maximum momenta in the range between 100 and 225 GeV/c that could be derived from a primary proton beam of 450 GeV/c with the intensity between 10^{12} and 10^{13} protons per SPS spill. The beam is produced by protons impinging on a primary beryllium target and transported to the detector in an evacuated beam-line tuned to a freely adjustable beam momentum [41]. The typical maximal intensity for a beam energy $\simeq 100$ GeV, is of the order of $5 \times 10^7 \mu^-$ for the SPS spill with 10^{12} protons on target. The typical SPS cycle for fixed-target (FT) operation lasts 14.8 s, including 4.8 s spill duration. The maximal number of FT cycles is four per minute. The hadron contamination in the muon

beam is remarkably negligible (below $\pi/\mu \lesssim 10^{-6}$) and the size of the beam at the detector position is of the order of a few cm^2 .

The detector shown in Fig. 4 utilizes two, upstream and downstream, magnetic spectrometers (MS) consisting of dipole magnets and a low-material budget tracker, which is a set of straw-tubes chambers, ST1-ST4 and ST5-ST8, allowing for the reconstruction and precise measurements of momenta for incident and scattered muons, respectively. It also uses scintillating fiber hodoscopes: S1 and S2 define the primary muon beam, while S3 defines the scattered muons, with the active target T surrounded by a high-efficiency electromagnetic calorimeter (ECAL) serving as a veto against photons and other secondaries emitted from the target at large angles. Downstream of the target the detector is equipped with high-efficiency forward veto counters V1 and V2 with small central holes, and a massive, completely hermetic hadronic calorimeter (HCAL) located at the end of the setup. The HCAL has four modules, each with lateral and longitudinal segmentation. The central part of the first (last) module is a cell with the lateral size $\simeq 100 \times 100 \text{ mm}^2$ ($\simeq 400 \times 400 \text{ mm}^2$), used to detect scattered muons and secondaries emitted in the very forward direction. It is also used for the final-state muon identification. The rest of each HCAL module serves as a dump to completely absorb and detect the energy of secondary particles produced in the muon interactions $\mu^- A \rightarrow \text{anything}$ in the target. The size of the central cells, straw-tube chambers ST9-ST12 and the counter S3 is determined by the requirement to keep the acceptance for deflected scattered muons with momentum in the range 15-100 GeV $\gtrsim 90\%$. For example, the lateral size of the S3 counter should be at least $50 \times 50 \text{ cm}^2$ and is determined mostly by the deflection angle in the second magnet and multiple scattering in the HCAL modules of scattered muons.

In order to suppress background due to the detection inefficiency, the HCAL must be longitudinally completely hermetic. To enhance its hermeticity, the HCAL thickness is chosen to be $\simeq 30 \lambda_{int}$ (nuclear interaction lengths). For searches at low energies, Cherenkov counters to enhance the incoming muon tagging efficiency can be used.

The method of the search is as follows. The bremsstrahlung Z_μ s are produced in the reaction (11) which occurs uniformly over the length of the target. A fraction (f) of the primary beam energy $E'_\mu = f E_\mu$ is carried away by the scattered muon which is detected by the second magnetic spectrometer, as shown in Fig. 4, tuned for the scattered muon momentum $p'_\mu \lesssim f p_\mu$. The remaining part of the primary muon energy $(1-f)E_\mu$ is transmitted through the HCAL by the neutrino from the prompt $Z_\mu \rightarrow \nu\nu$ decay resulting in a zero-energy deposition signal in the detector, i.e. in missing energy $E_{miss} = E_\mu - E'_\mu$.

The occurrence of Z_μ produced in $\mu^- Z$ interactions would appear as an excess of events with a single scattered muon accompanied by zero-energy deposition in the detector, as shown in Fig. 4, above those expected from the background sources. The signal candidate events have the signature:

$$S_{Z_\mu} = S1 \cdot S2 \cdot T \cdot \mu_{out} \cdot \overline{V1 \cdot V2 \cdot HCAL} \quad (34)$$

and should satisfy the following selection criteria:

- (i) $S1 \cdot S2 \cdot T$: The presence of an incoming muon with energy 150 GeV. The energy deposited in the target is consisted with that expected from the minimum ionizing particle (MIP).
- (ii) μ_{out} : The presence of a single scattered muon with energy $E'_\mu \lesssim 100$ GeV after the target, and the presence of a single muon track in the straw-tube chambers ST9-ST12 traversing the four HCAL modules.
- (iii) $\overline{V1 \cdot V2 \cdot HCAL}$: No energy deposition in the veto counters V1 and V2, no energy deposition in the central HCAL cells above those expected from the scattered muon, and no energy in the rest of the HCAL modules.

The "zero-energy" signal is defined by the following

- (i) The presence of the energy E_{ECAL}^μ deposited in the target, which is consistent with that deposited by the MIP.
- (ii) The presence of energy E_{HCAL}^μ deposited in the HCAL cell crossing by the scattered muon compatible with that expected from the MIP, $E_{HCAL}^\mu \simeq E_{mip}$, see Fig. 5. The primary muons that do not interact in the target and pass the HCAL without interactions deposit about (2.5 ± 1) GeV in each central cell.

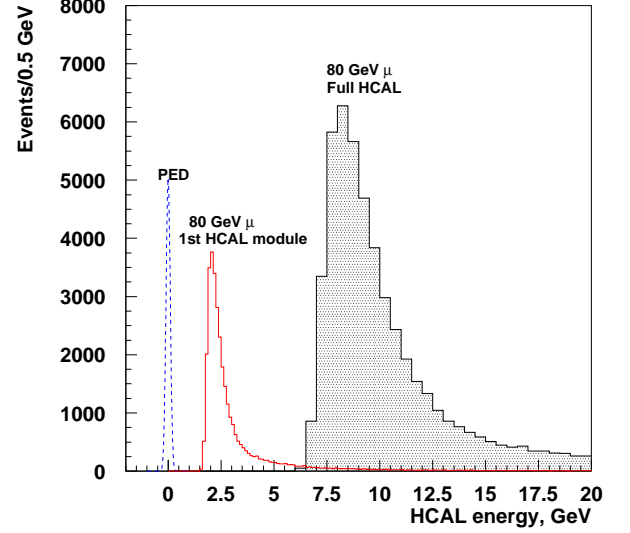


FIG. 5: The distribution of the energy deposited in the central cell of the first HCAL module (red histogram) and in all four HCAL central cells (shaded histogram) by traversing muons with energy $E_\mu = 80$ GeV. The peak of the pedestal sum over the rest of the HCAL in units of hadronic energy is also shown.

- (iii) No energy deposition in the veto counters V1 and V2, and in the rest of the HCAL, $E_{HCAL} \lesssim 100$ MeV, presented by the sum of pedestals of the read-out system, as shown in Fig. 5. The effective width of the signal in the rest of the HCAL is $\simeq 100$ MeV.
- (iv) The total energy deposited in the ECAL and HCAL is $E_{tot} = E_{ECAL} + E_{HCAL} \lesssim 12$ GeV.

The optimal primary beam energy is selected using the following considerations. First, it has to be high enough to provide the highest rate for the production of Z_μ 's in the sub-GeV mass range; second, it should correspond to as large an absolute value of E_{miss} as possible; and third, it should allow one to operate muon beam at high intensity. Taking these considerations into account, a beam energy around $\simeq 150$ GeV is chosen.

In Fig. 6, the simulated distribution of the events from the bremsstrahlung, knock-on, pair-production and photonuclear muon interactions in the target in the $(E'_\mu; E_{tot})$ plane is shown for the primary muon beam energy $E_\mu = 150$ GeV and a total number of incident muons $n_\mu \simeq 3 \times 10^8$ (see Sec.V). The events are selected with the requirement of no energy deposition in the veto counters V1 and V2. The signal of the reaction $\mu + Z \rightarrow \mu + Z + Z_\mu$, $Z_\mu \rightarrow \nu\nu$ is defined by a scattered muon energy of $E'_\mu \lesssim 100$ GeV and a total energy $E_{tot} = E_{ECAL} + E_{HCAL} \lesssim 12$ GeV. The width of the signal region along the E_{tot} axis corresponds to an energy deposition around 2.4 GeV in each central cell of four consecutive HCAL modules, as illustrated in Fig. 5,

plus about 0.5 GeV deposited in the ECAL, i.e. around 10 GeV for the total energy.

V. BACKGROUND

To estimate the background and sensitivity of the proposed experiment, a simplified feasibility study based on GEANT4 [42] Monte Carlo simulations has been performed for incoming muons with an energy of 150 GeV. In these simulations the target is the radiation-hard shashlik module ($X_0 \simeq 1.5$ cm) with a total thickness of about 50 X_0 , surrounded by the ECAL, which is a hodoscope array of the lead-scintillator counters that are also of the shashlik type, each with a size of $38 \times 38 \times 400$ mm³, allowing for accurate measurements of the lateral energy leak from the target. The shashlik calorimeter is a sampling calorimeter in which scintillation light is read out through wavelength-shifting fibers running perpendicular to the absorber plate; see, e.g. Ref. [43]. The target module consists of 300 layers of 1 mm thick lead and 1 mm thick plastic scintillator plates and has longitudinal segmentation.

Each of the scintillator counters S1, S2, and S3 consists of two layers of scintillating fiber strips, arranged in the X and Y directions, respectively. Each strip consists of about 100 fibers of 1 mm square. The number of photoelectrons produced by a MIP crossing the strip is $\simeq 20$ photoelectrons. The veto counters are assumed to be 1-2 cm thick, high-sensitivity scintillator arrays with a high light yield of $\gtrsim 10^2$ photoelectrons per 1 MeV of deposited energy. It is also assumed that the veto inefficiency for the MIP detection is, conservatively, $\lesssim 10^{-4}$. The hadronic calorimeter is a set of four modules. Each module is a sandwich of alternating layers of iron and scintillator with a thickness of 25 mm and 4 mm, respectively, and with a lateral size 120×120 cm². Each module consists of 48 such layers and has a total thickness of $\simeq 7\lambda_{int}$. The number of photoelectrons produced by a MIP crossing the module is in the range $\simeq 150$ -200 photoelectrons. The energy resolution of the HCAL calorimeters as a function of the beam energy is taken to be $\frac{\sigma}{E} \simeq \frac{60\%}{\sqrt{E}}$ [45]. The energy threshold for zero energy in the HCAL is $\simeq 0.1$ GeV. We assume that the momenta of the in- and outgoing muons are measured with a precision of a few percent. The scattered muon produced in the target is defined as a single track crossing the HCAL and the straw-tube stations ST9-ST12 and accompanied by no activity in the HCAL modules. The background reactions resulting in the signature of Eq. (34) can be classified as being due to physical- and beam-related sources. To investigate these backgrounds down to the level $\lesssim 10^{-10}$ with the full detector simulation would require a prohibitively large amount of computer time. Consequently, only the following background sources - identified as the most dangerous- are considered and evaluated with reasonable statistics combined with numerical calculations:

- One of the main background sources is related to the low-energy tail in the energy distribution of beam muons. The muon energy is lost due to the interaction of the particles with passive material, such as, e.g., entrance windows and the residual gas of beam lines. Another source of low-energy muons is due to the in-flight decays of pions and kaons that contaminate the beam. The uncertainties arising from the lack of knowledge of the dead material composition in the beam line are potentially the largest source of systematic uncertainty in accurate calculations of the fraction and energy distribution of these events. An estimation shows that the fraction of events with energy below $\lesssim 100$ GeV in the muon beam tuned to 150 GeV could be as large as 10^{-7} . Hence, the sensitivity of the experiment could be determined by the presence of such muons in the beam, unless one takes special measures to suppress this background.

To improve the high-energy muon selection and suppress the background from the possible admixture of low-energy muons, an additional tagging system utilizing a magnetic spectrometer is used, as schematically shown in Fig. 4. The precision of the muon momentum measurement with four straw-tube chambers is dominated by the track measurement errors $\sigma(x)(\simeq 100$ mkm) and is given by [44]

$$\frac{\sigma(p)}{p} \simeq \frac{\sigma(x)[m] \cdot 8p[GeV]}{0.3B[T](L[m])^2} \quad (35)$$

where B and L are the field strength and length of the magnet. The contribution from muon multiple scattering is negligible. Taking into account that $B \simeq 2$ T, and $L \simeq 2$ m results in $\frac{\sigma(p)}{p} \simeq 3\%$ for muons with momentum $p = 100$ GeV. Thus, the probability for a muon with $p \lesssim 100$ GeV to be taken as a 150 GeV one corresponds to the $\gtrsim 15$ sigma level and is negligible. The overall suppression of this background by the H4 beam-line spectrometer combined with this additional one is expected to be at a level much below 10^{-13} per incident muon.

- The low-energy muons could appear in the beam after the target due to the in-flight $\pi \rightarrow \mu\nu$ decay of the punch-through 150 GeV pions in the region between the tracker stations ST3 and ST4. In this case the pion could mimic the primary muon, while the decay muon could be taken as a fake scattered muon. Taking into account that the admixture of the pion in the beam is at the level $P_\pi \lesssim 10^{-6}$ [40] and the probability for the pion to decay at a distance of 4 m between the two spectrometers $P_d \sim 5 \times 10^{-4}$ results in an overall expected background at the level of 5×10^{-10} per incoming muon. To suppress this background further, one can use a cut that requires the maximal scattered muon en-

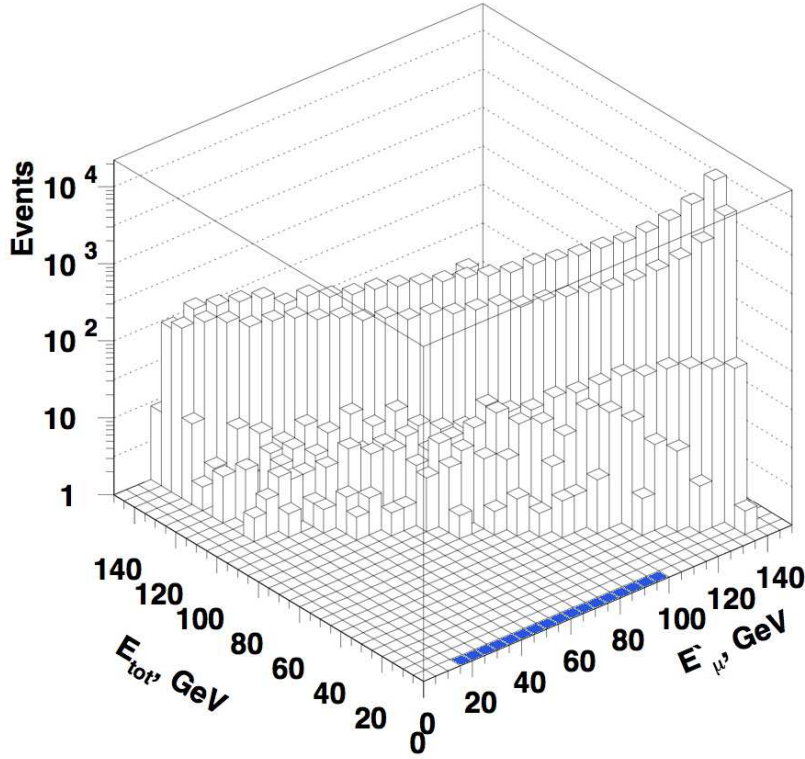


FIG. 6: Simulated distribution of events in the $(E'_\mu; E_{tot})$ plane from the bremsstrahlung, knock-on, pair-production and photonuclear muon interactions in the target that passed the veto selection criteria (v). The primary muon beam energy is $E_\mu = 150$ GeV and the total number of incident muons is $n_\mu \simeq 3 \times 10^8$. The blue area shows the signal of the reaction $\mu + Z \rightarrow \mu + Z + Z_\mu, Z_\mu \rightarrow \nu\nu$: the scattered muon energy $15 \lesssim E'_\mu \lesssim 100$ GeV and $E_{tot} = E_{ECAL} + E_{HCAL} \lesssim 12$ GeV.

ergy to be below the minimal kinematically allowed decay muon energy $E_{min}^\mu \simeq 86$ GeV.

However, in order to keep the muon efficiency as high as possible and still use the 15-100 GeV signal window shown in Fig.6, one can reduce the hadron contamination in the muon beam by utilizing an additional hadron absorber installed in the upstream part of the beam line. Using of a ~ 300 cm thick beryllium filter, which has the optimal ratio of $\lambda_{int}(\simeq 40 \text{ cm})/X_0(\simeq 35 \text{ cm})$, results in an additional reduction of the π/μ ratio down to $P_\pi \lesssim 10^{-9}$, at the cost of a small muon flux attenuation and an increase of the average multiple scattering angle. The combined probability for the $\pi \rightarrow \mu\nu$ decay background is then $P_\pi P_{dec} P_{cut} \lesssim 10^{-13}$, where $P_{cut} \lesssim 0.2$ is a probability for decay muon to have momentum $P_\mu \lesssim 100$ GeV.

- The fake signature of Eq.(34) could also arise when a high-energy muon loses energy through hard bremsstrahlung (BR), knock-on electrons (KN), pair-production (PP) or photonuclear (PN) inter-

actions in the target. The fraction of these reactions, compared with the total muon energy losses including ionization losses, depends on the ratio E'_μ/E_μ and for the Pb target is in the range $\simeq 10^{-3} - 10^{-5}$ per X_0 for $0.1 \lesssim E'_\mu/E_\mu \lesssim 0.9$ [46]. Such reactions could yield a low-energy scattered muon accompanied by neutral penetrating particles in the final state (e.g. photons, neutrons, K_L^0 , etc.), which then could escape detection in the rest of the detector. Simulations show that in this case, the background is dominated by the photonuclear reactions accompanied by the emission of hadrons or a leading hadron h from the muon-induced reactions $\mu A \rightarrow \mu h X$ which could escape detection due to incomplete hermeticity of the HCAL. For the energy range discussed the muon photonuclear cross section is $\sigma_{PN}(\mu N \rightarrow \mu X) \simeq 10^{-2} \sigma_{tot}$ of the total interaction cross section $\sigma_{tot} = \sigma_{BR} + \sigma_{KN} + \sigma_{PP} + \sigma_{PN}$ [46]. This important source of background was examined by using several methods.

- In Fig. 7 we show the simulated distribution of the energy deposited in the (ECAL+HCAL) by sec-

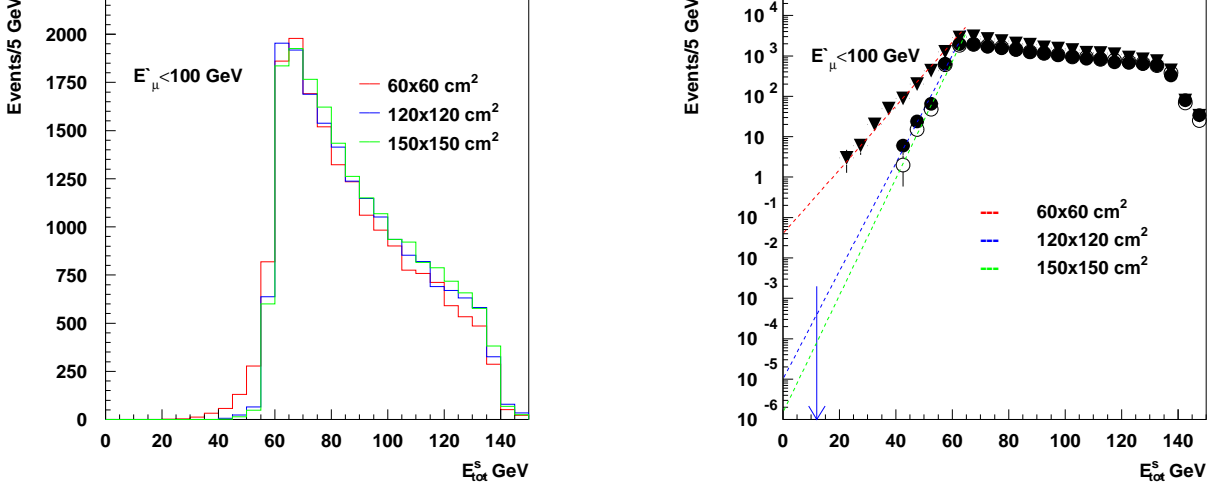


FIG. 7: The l.h.s. shows the simulated distribution of the energy deposited in the ECAL+HCAL by secondaries from the bremsstrahlung, pair-production, knock-on and photonuclear muon interactions in the target. The events are selected by requiring the presence of a scattered muon crossing the central HCAL cells with initial energy $E'_\mu \lesssim 100$ GeV and no energy deposition in the veto counters V1 and V2. The energy ($E_{ECAL}^\mu + E_{HCAL}^\mu$) deposited by the scattered muon in the ECAL and the HCAL central cells is subtracted. On the r.h.s. the same distribution (dots) is shown on a logarithmic scale. Other plots correspond to the energy distribution in the ECAL+HCAL for the HCAL with half of the lateral size, i.e., 60×60 cm² (triangles) and 150×150 cm² (open circles). The curves are the fit of the low-energy tail of the distributions by a smooth polynomial function extrapolated to the signal region $E_{tot}^s = E_{ECAL} + E_{HCAL} - E_{ECAL}^\mu - E_{HCAL}^\mu \lesssim 12$ GeV, indicated by the arrow, in order to conservatively evaluate the expected number of background events. The importance of the HCAL transverse size for the minimization of the lateral leak of the energy and the reduction of the number of background events is clearly seen.

ondaries from the bremsstrahlung, knock-on, pair-production or photonuclear muon interactions in the target. The events are selected by requiring additionally the presence of a scattered muon crossing the central HCAL cells with an energy $E'_\mu \lesssim 100$ GeV and no energy deposition in the veto counters V1 and V2. The energy deposited by the scattered muon in the ECAL and the HCAL central cell is subtracted. The low-energy tail of this distribution was fitted by a smooth polynomial function and extrapolated to the energy region $E_{tot}^s \lesssim 12$ GeV to evaluate the number of background events in the signal region. Those events with an energy deposition below the typical energy deposited by the MIP could mix with the muon signal resulting in the fake signal. Using this rough estimate we find that this background is expected to be at the level $\lesssim 10^{-12}$ per incoming muon. IN the same plot the distribution of the energy in the ECAL+HCAL for the HCAL with half the lateral size, i.e. 60×60 cm² and 150×150 cm² are shown for comparison. The effect of the HCAL transverse size on the lateral leak of the energy deposition from the bremsstrahlung, pair-production, knock-on or photonuclear muon interactions in the target and the corresponding number of background events is clearly seen.

- Another method is based on the direct estimate of the probability for the large missing energy in

the detector. The energy could also leak when the leading neutron or K_L^0 punches through the HCAL without depositing energy above a certain threshold E_{th} . In this case, if the sum of the energy released in the HCAL is below E_{th} , the event is considered as a "zero-energy" event. The punch-through probability P_{pth} is defined roughly by $P_{pth} \simeq \exp(-L_{tot}/\lambda_{int})$, where L_{tot} is the HCAL length. As discussed previously, it can be suppressed by using the HCAL with a thickness of $\simeq 30\lambda_{int}$, resulting in a P_{pth} of $\ll 10^{-10}$. This value should be multiplied by a conservative factor $\lesssim 10^{-4}$, which is the probability of a single leading hadron production in the target, resulting in the final estimate of $\lesssim 10^{-13}$ for the level of this background per incoming muon.

- For completeness, the HCAL nonhermeticity and corresponding background for high-energy secondary hadrons were cross-checked with GEANT4-based simulations in the following way. In Fig. 8 we show the expected distributions of energy deposited by $\simeq 10^6$ K^0 with energy $\simeq 95$ GeV in two (a) and four (b) consecutive HCAL modules. The peak at zero energy in the spectrum (a) is due to the punch-through neutral kaons, while for the full HCAL thickness there are no such missing energy events in distribution (b).

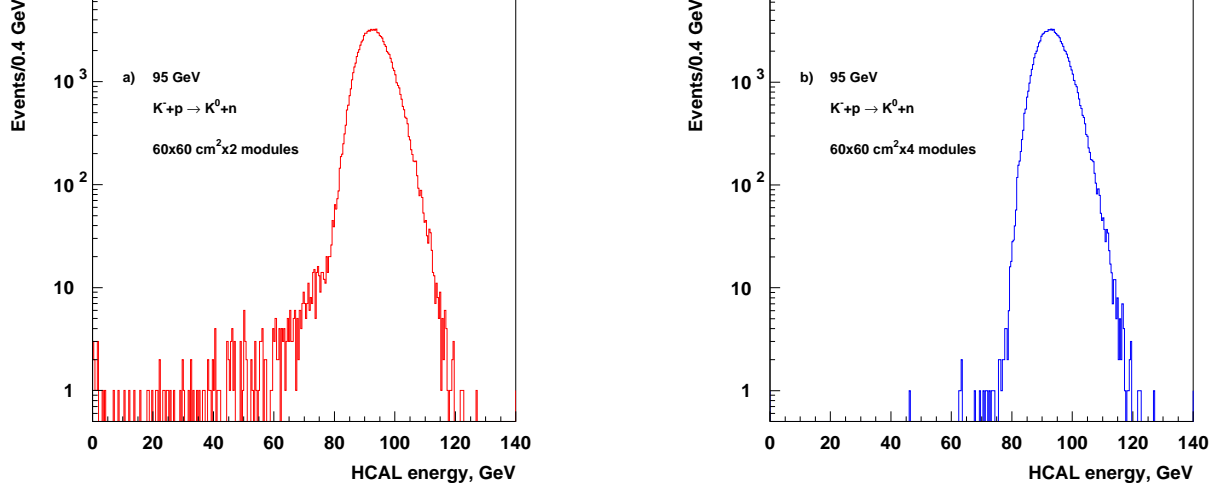


FIG. 8: Expected distributions of energy deposited by $\simeq 10^6$ K^0 with energy $\simeq 95$ GeV in two (a) and four (b) consecutive HCAL modules. The peak at zero energy in spectrum (a) is due to the punch-through neutral kaons.

For another sample of simulated events, the low-energy tail in the distribution of energy deposited by $\simeq 10^7$ 150 GeV neutrons in the HCAL was fitted by a smooth polynomial function and extrapolated to the lower-energy region in order to evaluate the number of events below a certain threshold E_{th} . This procedure results in an estimate for the HCAL nonhermeticity, defined as the ratio of the number of events below the threshold E_{th} to the total number of incoming particles: $\eta = n(E < E_{th})/n_{tot}$. For the energy threshold $E_{th} \simeq 0.1$ GeV the nonhermeticity is expected to be at the level $\eta \lesssim 10^{-9}$. Taking into account a probability of producing a single leading hadron per incoming muon of $P_h \lesssim 10^{-4}$, results in an overall level of this background of $\lesssim 10^{-13}$, in agreement with the previous rough estimate.

- The fake signature of Eq. (34) could be due to the QED production of muon trident events, $\mu Z \rightarrow \mu Z \mu^+ \mu^-$, with asymmetrical muon momenta in the muon pair. In this case, the lower-energy muon could be poorly detected, and another one could admix to the scattered muon in the HCAL central cell. A preliminary simulation study shows that this background can be suppressed down to the 10^{-12} level, provided the inefficiency of veto counters V1 and V2 is below 10^{-4} and the two tracks separated by a distance $\simeq 1$ mm are resolved by the ST5-ST8 and ST9-ST12 trackers.

In Table I contributions from the all dominant background processes are summarized for a primary muon beam energy of 150 GeV. The total background is found to be at the level $\lesssim 10^{-12}$. The contribution of additional subdominant background sources (e.g., such as

very asymmetric $\mu \rightarrow e \nu \nu$ decays accompanied by low-energy muon production in the HCAL by the decay electron, cosmic muons, etc.) is negligible. This means that the search accumulated up to $\simeq 10^{12}$ μ^- events is expected to be background free.

TABLE I: Expected contributions to the total level of background from different background sources estimated for a beam energy of 150 GeV (see text for details).

Source of background	Expected level
μ low-energy tail	$\lesssim 10^{-13}$
HCAL nonhermeticity	$\lesssim 10^{-13}$
μ induced photonuclear reactions	$\lesssim 10^{-13}$
μ trident events	$\lesssim 10^{-12}$
Total	$\lesssim 10^{-12}$

VI. EXPECTED SENSITIVITY

To estimate the expected sensitivities we used simulations of the process shown in Fig. 4 to calculate the production rate and energy distributions of muons produced in the target by taking into account the normalization of the scattered muon yield from the target taken from the original publications [46]. The calculated fluxes and energy distributions of scattered muons produced in the target are used to predict the number of signal events in the detector. For a given total number of primary muons n_μ , the expected number of events from the reaction $\mu + Z \rightarrow \mu + Z + Z_\mu, Z_\mu \rightarrow \nu \nu$ occurring within the

decay length L of the detector is given by

$$n_{Z_\mu} = kn_\mu Br(Z_\mu \rightarrow \nu\nu) \frac{\rho N_A}{A} \cdot \int \frac{\sigma(\mu+Z \rightarrow \mu+Z+Z_\mu)}{dx} d\zeta(M_{Z_\mu}) dx \quad (36)$$

with $d = 1$ for $M_{Z_\mu} < 2m_\mu$, and $d = \left[1 - \exp\left(-\frac{LM_{Z_\mu}}{P_{Z_\mu}\tau_{Z_\mu}}\right)\right]$ for $M_{Z_\mu} > 2m_\mu$. Here, the coefficient k is a normalization factor that was tuned to obtain the total cross sections of meson production, P_{Z_μ} and τ_{Z_μ} are the produced Z_μ momentum and lifetime at rest, respectively, $\zeta(M_{Z_\mu})$ is the overall signal reconstruction efficiency, ρ is the density of the target, L is the decay length in the detector, and N_A is the Avogadro number. In this estimate we neglect the scattered μ interactions in the target, the momentum of the incoming muons is $\langle p_\mu \rangle \simeq 150$ GeV, and the efficiency $\zeta(M_{Z_\mu})$ is in the range $\simeq 0.1 - 0.5$ for the masses $1 \text{ MeV} \lesssim M_{Z_\mu} \lesssim O(5) \text{ GeV}$.

The obtained results can be used to impose constraints on the previously discussed coupling strength α_μ as a function of the Z_μ mass. Using the relation $n_{Z_\mu}^{90\%} > n_{Z_\mu}$, where $n_{Z_\mu}^{90\%}$ ($= 2.3$ events) is the 90% *C.L.* upper limit for the number of signal events and Eq. (36), one can determine the expected 90% *C.L.* upper limits from the results of the proposed experiment, which are shown in Fig. 9 together with values of the coupling α_μ required to explain the muon $g-2$ anomaly. These bounds are calculated for a scattered muon energy $10 \lesssim E'_\mu \lesssim 100$ GeV and a total of 10^{12} incident muons in the background-free case. Here we assume an exposure to the muon beam with a nominal rate is a few months.

The statistical limit on the sensitivity of the proposed experiment is mostly set by the number of accumulated events. However, there is a limitation factor related to the HCAL signal duration ($\tau_{HCAL} \simeq 100$ ns) resulting in a maximally allowed muon counting rate of $\lesssim 1/\tau_{HCAL} \simeq 10^6 \mu^-/s$ in order to avoid significant loss of the signal efficiency due to the pileup effect. To evade this limitation, one could implement a special muon pileup removal algorithm to allow for high-efficiency reconstruction of the zero-energy signal properties and the shape in high muon pileup environments, and run the experiment at the muon beam rate $\simeq 1/\tau_{HCAL} \simeq 10^7 \mu^-/s$. Thus, in the background-free experiment one could expect a sensitivity in the process $\mu + Z \rightarrow \mu + Z + Z_\mu$, $Z_\mu \rightarrow \nu\nu$ that is even higher than those presented above, assuming an exposure to the high-intensity muon beam of a few months. In the case of the Z_μ signal observation, several methods could be used to cross-check the result. For instance, to test whether the signal is due to the HCAL nonhermeticity or not, one could perform measurements with different HCAL thicknesses, i.e., with one, two, three, and four consecutive HCAL modules. In this case the background level can be evaluated by extrapolating the results to an infinite HCAL thickness. To insure that there is no additional background due to the HCAL transverse hermeticity one could perform measurements for differ-

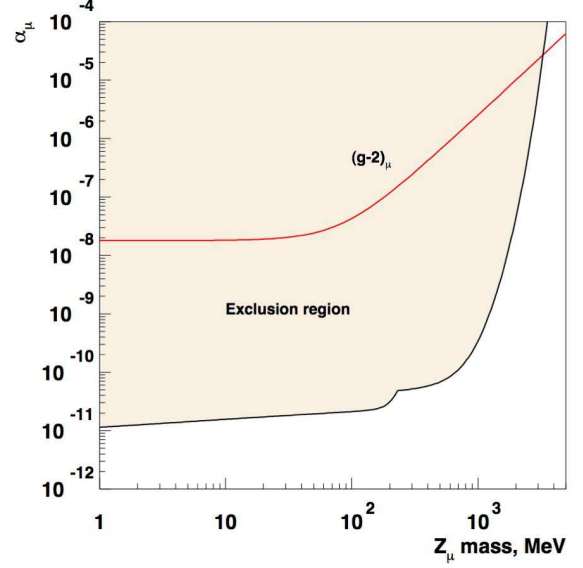


FIG. 9: Exclusion region in the (M_{Z_μ}, α_μ) plane expected from the results of the proposed experiment for 10^{12} incident muons at the energy $E_\mu = 150$ GeV. The red line represents the value of α_μ required to explain the muon $g-2$ discrepancy as a function of the Z_μ mass.

ent distances between the target and the HCAL. The evaluation of the signal and background could also be obtained from the results of measurements at different muon beam energies. Finally, we note that the presented analysis gives an illustrative order of magnitude for the sensitivity of the proposed experiment and may be strengthened by more detailed simulations of the experimental setup.

VII. CONCLUSION

In this work we considered the discrepancy between the measured and predicted values of the muon $g-2$ which could be explained by the existence of a new light gauge boson Z_μ predominantly coupled to the second and third generations. We proposed performing an experiment dedicated to the sensitive search for the Z_μ by using available $\simeq 100$ GeV muons beams from the CERN SPS. If the Z_μ s exist, they could be produced in the reaction $\mu + Z \rightarrow \mu + Z + Z_\mu$ and be observed by looking for events with a specific signature, namely those missing a large fraction of the beam energy in the detector. A feasibility study of the experimental setup shows that this specific signal of the Z_μ allows for searches for the Z_μ with a sensitivity in the coupling constant $\alpha_\mu \gtrsim 10^{-11}$, i.e., 3 orders of magnitude stronger than the value $\alpha_\mu \sim 10^{-8}$ explaining the 3.6σ muon $g-2$ discrepancy for the Z_μ mass range $M_{Z_\mu} < O(5) \text{ GeV}$ [5].

These results could be obtained with a detector opti-

mized for several of its properties, namely, i) the intensity and purity of the primary pion and kaon beams, ii) the high efficiency of the veto counters, and iii) the high level of hermeticity for the hadronic calorimeters. Large amount of high-energy muons and high background suppression are crucial for improving the sensitivity of the search. To obtain the best limits, the choice of the energy and intensity of the beam, as well as the background level should be compromised.

We point out that the availability of high-energy and -intensity muon beams at CERN SPS provides a unique opportunity to either discover or rule out the Z_μ with

the proposed search in the near future. The experiment is based on the missing-energy approach developed for the searches for invisible decays of dark photons and (pseudo)scalar mesons at CERN [12–14] and is complementary to these experiments. It also provides interesting motivations for further muon studies and fits well with the present muon physics program at CERN.

Acknowledgments

The help of M. Kirsanov and A. Toropin in calculations is greatly appreciated. The work is supported by RFBR grant 13-02-00363.

-
- [1] G.W.Bennett et al., [Muon G-2 Collaboration], Phys.Rev. D **73**, 072003 (2006).
 - [2] A.Czanecki and W.J.Marciano, Phys. Rev. D **64**, 013014 (2001); L.Everett, G.L.Kane, S.Rigolin and L.-T.Wang, Phys.Rev.Lett. **86**, 3484 (2001); J.L.Feng and K.T.Matchev, Phys.Rev.Lett. **86**, 3480 (2001); E.A.Baltz and P.Gondolo, Phys.Rev.Lett. **86**, 5004 (2001); U.Chattopadhyay and P.Nath, Phys.Rev.Lett. **86**, 5854 (2001).
 - [3] U.Mahanta, Eur. Phys. J. C **21**, 171 (2001); D.Chakraverty, D.Choudhury and A.Datta, Phys. Lett. B **506**, 103 (2001); F.S. Queiroza, K. Sinhab and A. Strumia, Phys. Rev. D **91**, 035006 (2015).
 - [4] T.Huang, Z.-H.Lin, L.-Y. Shan, and X.Zhang, Phys. Rev. D **64**, 071301 (2001); D.Choudhury, B.Mukhopadhyaya and S.Rakshit, Phys. Lett. B **507**, 219 (2001).
 - [5] S.N.Gninenko and N.V.Krasnikov, Phys. Lett. B **513**, 119 (2001).
 - [6] S.Baek et al., Phys. Rev. D **64**, 055006 (2001).
 - [7] E.Ma, D.Roy and S.Roy, Phys. Lett. B **525**, 101 (2002).
 - [8] P.Fayet, Phys. Rev. D **75**, 115017 (2007).
 - [9] M.Pospelov, Phys. Rev. D **80**, 095002 (2009).
 - [10] J.Heeck and W.Rodejohann, Phys. Rev. D **84**, 075007 (2011).
 - [11] C.D. Carone, Phys. Lett. B **721**, 118 (2013); arXiv:1301.2027 [hep-ph].
 - [12] S.N. Gninenko, Phys. Rev. D **89**, 075008 (2014); arXiv:1308.6521 [hep-ph].
 - [13] S. Andreas et al., arXiv:1312.3309 [hep-ex].
 - [14] S.N. Gninenko, Phys. Rev. D **91**, 015004 (2015).
 - [15] B.Holdom, Phys. Lett. B **178**, 65 (1986).
 - [16] K.R.Dienes, C.F.Kolda, and J.March-Russell, Nucl. Phys. B **492**, 104 (1997).
 - [17] H.Davoudiasl, H.S.Lee, and W.J.Marciano, Phys. Rev. D **86**, 095009 (2012).
 - [18] M.Endo, K.Hamaguchi, and G.Mishima, Phys. Rev. D **86**, 095029 (2012).
 - [19] A.Adare et al. (Phenix Collaboration), Phys. Rev. C **91**, 031901 (2015).
 - [20] H.Merkel et al. (A1 Collaboration), Phys. Rev. Lett. **112**, 221802 (2014).
 - [21] J.P.Lees et al. (BABAR Collaboration), Phys. Rev. Lett. **113**, 201801 (2014).
 - [22] F. Ambrosino et al., arXiv:1408.0585.
 - [23] Y.Kahn, G. Krnjaic, J. Thaler, and M. Toups, Phys. Rev. D **91**, 055006 (2015).
 - [24] A.V.Artamonov et al. (BNL-E249 Collaboration), Phys. Rev. D **79**, 092004 (2009).
 - [25] B.Aubert et al. [BABAR collaboration], arXiv:0808.0017.
 - [26] F.Izzaguirre et al. Phys. Rev. D **88**, 114015 (2013); R.Essig et al., JHEP bf 11, 167 (2013).
 - [27] H.-S. Lee, Phys. Rev. D **90**, 091702 (2014).
 - [28] D.Geiregat et al. [CHARM-II Collaboration], Phys. Lett. B **245**, 271 (1990).
 - [29] S.R.Mishra et al.[CCFR Collaboration], Phys. Rev. Lett. **66**, 3117 (1991).
 - [30] J.D. Bjorken et al., Phys. Rev. D **38**, 3375 (1988).
 - [31] E. M. Riordan et al., Phys. Rev. Lett. **59**, 755 (1987).
 - [32] A. Bross, M. Crisler, S. H. Pordes, J. Volk, S. Errede, and J. Wrbanek, Phys. Rev. Lett. **67**, 2942 (1991).
 - [33] G.Bellini et al., Phys.Rev.Lett. **107**, 141302 (2011).
 - [34] R.Harnik, J.Kopp and P.A.N.Machado, JCAP **07**, 026 (2012); R.Laha, B.Dasgupta and J.F.Beacom, Phys. Rev. D **89**, 093025 (2014).
 - [35] R. Foot, Mod. Phys. Lett. A **06**, 527 (1991); R. Foot, X. G. He, H. Lew, and R.R. Volkas, Phys. Rev. D **50**, 4571 (1994); X.-G. He, G. C. Joshi, H. Lew, and R. Volkas, Phys. Rev. D **43**, R22 (1991); X.-G. He, G. C. Joshi, H. Lew, and R. Volkas, Phys. Rev. D **44**, 2118 (1991).
 - [36] T. Araki, F. Kaneko, Y. Konishi, T. Ota, J. Sato, T. Shimomura, Phys. Rev. D **91**, 037301 (2015).
 - [37] W.Almannsofer, S.Gori, M.Pospelov and I.Yavin, Phys.Rev.Lett. **113** 091801 (2014); arXiv:1406.2322.
 - [38] See, for instance, Y.-S.Tsai, Rev. Mod. Phys. **46**, 815 (1974); Y.-S.Tsai, Phys. Rev. D **34**, 1326 (1986); K.J.Kim and Y.-S.Tsai, Phys. Rev. D **8**, 3109 (1973).
 - [39] J.D.Bjorken, R.Essig, P.Schuster and N.Toro, Phys. Rev. D **80**,075028 (2009); S.Andreas, G.Niebuhr and A.Ringwald, Phys. Rev. D **86**, 095019; E. Izaguirre, G. Krnjaic, P. Schuster, and N. Toro, arXiv:1411.1404.
 - [40] N. Doble, L. Gagnon, G. von Holtey, and F. Novoskoltsev, Nucl. Instrum. Meth. A **343**, 351 (1994).
 - [41] See, for example, <http://sba.web.cern.ch/sba/>
 - [42] S. Agostinelli et al. (GEANT4 Collaboration), Nucl. Instrum. Meth. A **506**, 250 (2003); J. Allison et al. (GEANT4 Collaboration) IEEE Trans. Nucl. Sc. **53**, 270 (2006).
 - [43] G.S. Atoian, V.A. Gladyshev, S.N. Gninenko, V.V.

- Isakov, A.V. Kovzelev, et al., Nucl. Instrum. Methods Phys. Res., Sect. A **320**, 144 (1992).
- [44] See, for example, C. Grupen and B. Shwartz, *"Particle Detectors"* (Cambridge University Press, Cambridge, England, 2008).
- [45] G.A. Alekseev et al., Nucl. Instrum. Methods Phys. Res., Sect. A **461**, 381 (2001).
- [46] D.E. Groom, N.V. Mokhov, and S.I. Striganov, At. Data Nucl. Data Tables **78**, 183 (2001).
- [47] E.D. Carlson, Nucl. Phys. B **286** 378 (1987).
- [48] M.I.Dobroliubov and A.Yu.Ignatiev, Nucl. Phys. **B309** 655 (1988), M.I. Dobroliubov, Yad. Phys. **52** 551 (1990) [Sov. J. Nucl. Phys. **52** 352 (1990)].
- [49] S.N.Gninenko and N.V.Krasnikov, Phys. Lett. B **427** 307 (1998).
- [50] L.B. Okun, Phys. Lett. B **382** 389 (1996).
- [51] For instance, for $m_{Z'} = 1$ MeV the experimental bounds on e' is $e' \leq 3 \times 10^{-6}$ [34]. Note that in the early papers [47]-[49] (see also Ref.[50]) similar bounds on the Z_μ -boson coupling from neutrino reactions were obtained.